

## A multi-model approach to intravenous filter optimization

Y. V. Vassilevski<sup>1,\*</sup>, S. S. Simakov<sup>2</sup> and S. A. Kapranov<sup>3</sup>

<sup>1</sup>*Institute of Numerical Mathematics RAS, 119333, Gubkina St. 8, Moscow, Russia*

<sup>2</sup>*Moscow Institute of Physics and Technology, 141700, Institutski Lane 9, Dolgoprudny, Russia*

<sup>3</sup>*Department of Interventional Radiology, City Hospital N 1, 117049, Leninskiy pr. 8, Moscow, Russia*

### SUMMARY

We present a multi-model approach to the study of side-effects of endovascular implants. A 2D model of elastic walls and a local 3D model of blood flow are combined with a 1D network blood circulation model. The three numerical models form an endovascular computational stand. Copyright © 2010 John Wiley & Sons, Ltd.

Received 30 November 2009; Revised 26 February 2010; Accepted 1 March 2010

KEY WORDS: blood flow; endovascular implants; cava filter optimization

### 1. INTRODUCTION

Development of endovascular devices is one of the most challenging problems in contemporary medicine. Millions of endovascular implants are successfully installed annually. The design and installation of the devices-implants should minimize perturbations of the blood flow in the vessel as well as the impact on the vessel wall. This requires optimization of the device structure, choice of appropriate materials, study of the place and the method of the device fixation, estimation of the impact on the global circulation, evaluation of chemical species transport in the case of dissoluble devices. Our work addresses modeling side-effects due to intravenous filters (Figure 1), which are implanted into veins to capture and dissolve migrating thrombi. In particular, we consider correct filter placement, computation of flow in the vicinity of the filter and captured thrombus, impact of the installed filter on the elastic properties of the venous wall, transport of polymeric material in case of dissoluble filter.

The cardiovascular models of different dimensions have been widely developed and discussed [1–4]. The tasks of fluid–structure interaction and multi-modeling are the main points in such works. Our approach to multi-modeling adopts the fluid–structure interaction using the immersed boundary method [5, 6] and fluid–network interaction using defective boundary conditions [7], and is genuine for the network–structure interaction. The key feature of the latter is the recovery of vessel’s wall state equation, which requires less computational resources and is simpler in adjustment from the point of averaged physiological data.

---

\*Correspondence to: Y. V. Vassilevski, Institute of Numerical Mathematics RAS, 119333, Gubkina St. 8, Moscow, Russia.

†E-mail: vassilevs@dodo.inm.ras.ru, yuri.vassilevski@gmail.com

Contract/grant sponsor: ISTC; contract/grant number: 3744

Contract/grant sponsor: RFBR; contract/grant number: 08-01-00159

Contract/grant sponsor: FCPK Research and Educational Personnel of Innovative Russia; contract/grant numbers: P727, P468, P1127

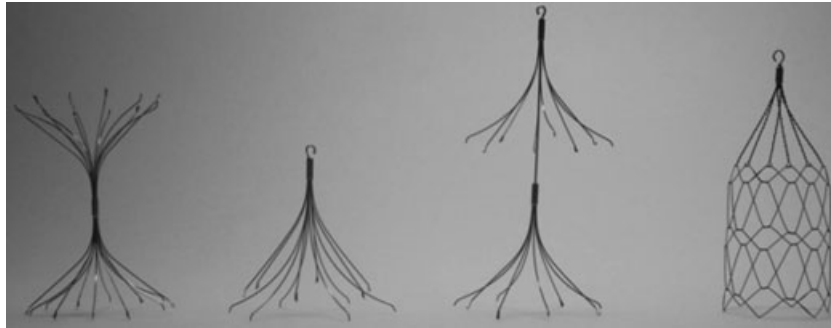


Figure 1. Samples of intravenous filters (Comed Co.).

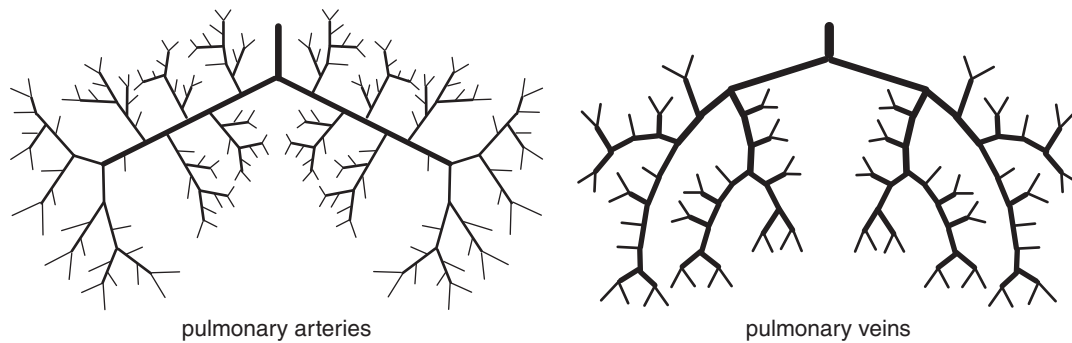


Figure 2. 1D structure of the pulmonary vessels.

## 2. METHODS

Three numerical models of different dimensionalities are proposed for the minimization of side-effects due to installation of intravenous implants. The detailed disturbance of the blood flow in the vicinity of the implant should be considered by means of 3D incompressible fluid flow model. Global response to the local perturbations should be analyzed in the scope of 1D network circulation model. The elastic vessel wall response to the device fixation and flow pulsations should be taken into account through the 2D model of elastic structures and fluid–structure interaction problem.

### 2.1. 1D network blood flow model

In the network circulation model, the domain is a set of 1D flexible channels connected in a closed network consisting of four parts (arterial and venous parts of the pulmonary and systemic circles) shown in Figures 2 and 3. The structure of the pulmonary network (Figure 2) was reconstructed on the basis of reported clinical investigations [8, 9]. Implementation of the systemic circulation structure (Figure 3) is more tedious. The data were gathered through a wide range of sources, e.g. [10, 11] etc.

Blood flow is considered as pulsating flow of incompressible fluid streaming through the network of elastic tubes (vessels). For every vessel we have mass and momentum conservation equations in the characteristic form [12–14]:

$$\partial S/\partial t + \partial(Su)/\partial x = \varphi(t, x, S, u, \chi_i), \quad (1)$$

$$\partial u/\partial t + \partial(u^2/2 + p/\rho)/\partial x = \psi(t, x, S, u, \chi_i), \quad (2)$$

where  $t$  is the time,  $x$  the coordinate along the vessel,  $\rho$  the blood density,  $S(t, x)$  the vessel cross-section area,  $u(t, x)$  the linear flow velocity averaged over the vessel cross section,  $p$  the

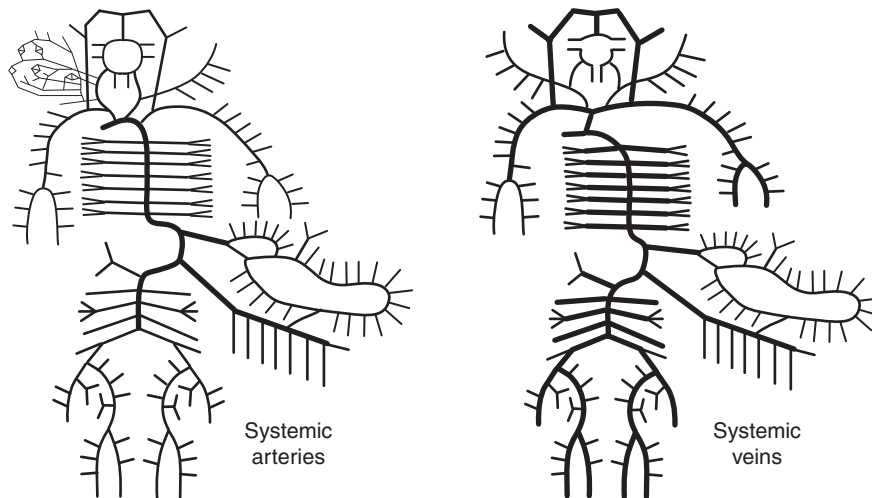


Figure 3. 1D structure of the systemic vessels.

pressure (relative to the atmospheric pressure),  $\varphi$  the mass inflow/outflow (e.g. due to the damage of the vessel wall or blood transfusion),  $\psi$  the external force (e.g. gravity, friction, etc.),  $\chi_i$  the parameter of the  $i$ th impact (loss of blood, external stress, etc.). The elastic properties of the vessel wall are described by the state equation defining the dependence of pressure  $p$  from the instant vessel cross-section area  $S$

$$p(S) = p_* + \rho c_0^2 f(S), \tag{3}$$

where  $c_0$  is the rate of small disturbance propagation in the vessel wall,  $p_*$  is the pressure in the tissues surrounding the vessel. The function  $f(S)$  depends on the type of the vessel. In this work we set for intact vessels (i.e. vessels without installed endovascular devices)  $S$ -like dependence [15] reported in many works. We use it in the following form [12, 14]:

$$f(S) = \begin{cases} \exp(S/\bar{S}) - 1, & S > \bar{S}, \\ \ln(S/\bar{S}), & S \leq \bar{S}, \end{cases} \tag{4}$$

where  $\bar{S}$  is the vessel cross-section area under zero transmural pressure  $p(S) - p_*$  and zero velocity.

All the vessels must be connected with each other at the nodes and to the heart by the appropriate boundary conditions that are formed by Poiseuille's pressure drop conditions and mass conservation law combined with the appropriate compatibility condition for (1), (2)

$$p_k(S_k(t, \tilde{x}_k)) - p_{\text{node}}^l(t) = \varepsilon_k R_k^l S_k(t, \tilde{x}_k) u_k(t, \tilde{x}_k), \quad k = k_1, k_2, \dots, k_M, \tag{5}$$

$$\sum_{k=k_1, k_2, \dots, k_M} \varepsilon_k S_k(t, \tilde{x}_k) u_k(t, \tilde{x}_k) = 0, \tag{6}$$

where  $l$  is the node's index,  $k$  the vessel index,  $k_1, k_2, \dots, k_M$  and  $M$  are the indexes and the number of the vessels meeting at the node;  $p_{\text{node}}^l(t)$  the pressure at the vessels junction point;  $R_k^l$  the hydraulic resistance for the flow from the  $k$ th vessel to the  $l$ th node. For branches incoming into a node (having terminal point near the node), we set  $\varepsilon_k = 1, \tilde{x}_k = L_k$ , whereas for outgoing branches (having entry point near the node), we set  $\varepsilon_k = -1, \tilde{x}_k = 0$ . In the case of the heart junction, the product  $S_k(t, x) u_k(t, x)$  in (5), (6) should be replaced with volumetric flow to or from the appropriate chamber of the heart  $Q_k$ .

### 2.2. Numerical implementation of 1D network blood flow model

For every vessel, Equations (1)–(4) are solved by the hybrid (first and second order) explicit grid-characteristic method. This model also includes a set of stiff ordinary differential equations

(ODEs), which describe the heart functioning in terms of the volume-averaged model [12]. The system of ODEs is solved by A- and L-stable implicit third-order Runge–Kutta method.

Finite-difference approximation of the compatibility condition for (1), (2) along the characteristic outgoing from the integration domain gives linear dependence  $u_k^{n+1}$  from  $S_k^{n+1}$  at the upper time layer  $n + 1$  (see [12, 14] for details)

$$u_k^{n+1} = \alpha_k S_k^{n+1} + \beta_k. \tag{7}$$

This allows us to reduce the nonlinear equations (5), (6) to the system of two times less dimension

$$\vec{F}(\vec{S}) = \Delta \vec{f} + \mathbf{R} \vec{P} = \vec{0}, \tag{8}$$

where

$$\vec{f} = \{\varepsilon_{k_m} (\alpha_{k_m} S_{k_m} + \beta_{k_m}) S_{k_m}\}_{m=1}^M, \quad \vec{P} = \{p_{k_m}\}_{m=1}^M, \tag{9}$$

$$\mathbf{R} = \{R_{ij}\}_{i,j=1}^M, \quad R_{ii} = - \sum_{\substack{j=1 \\ j \neq i}}^M \prod_{\substack{m=1 \\ m \neq i \\ m \neq j}}^M R_{k_m}^l, \quad R_{ij} = \prod_{\substack{m=1 \\ m \neq i \\ m \neq j}}^M R_{k_m}^l, \quad \Delta = \det \mathbf{R} = \sum_{i=1}^M \prod_{\substack{j=1 \\ j \neq i}}^M R_{k_j}^l, \tag{10}$$

$\mathbf{R}$  is a symmetric matrix describing the total node’s hydraulic resistance.

The numerical solution of the system (8) by the Newton method requires almost 10 times less operations than the numerical solution of (5), (6). Moreover, the Newton method demonstrates better convergence, particularly in the case of great diameter ratios for the vessels meeting at a node.

### 2.3. 2D elastic wall model

In the elastic wall model the domain is the two-dimensional manifold whose position in space can vary. The model of the elastic properties of the vessel wall is based on its fiber composition. The fibers produce the elastic strain that resists the deformation of the vessel. This approach was developed by Peskin and Tu [5] in the 2D case and by Peskin and Rosar [6] in the 3D case.

The wall is modeled as a set of elastic fibers. All fibers can be divided into three types: elastic, smooth muscle, and collagen. We set their Young’s modules to  $3 \times 10^5$ ,  $3 \times 10^5$ ,  $10^8 \text{ Nm}^{-2}$ , respectively. Collagen fibers are distributed in the wall in unstrained state and begin to respond to the deformation when the wall is considerably deformed.

The fibers are grouped according to geometric features. In accordance with the anatomic structure of the vessel, we separate ring, beam, and helical fibers and locate them so that they uniformly cover the wall of the vessel, see Figure 4.

### 2.4. Numerical implementation of 2D elastic wall model

In the numerical model, each fiber is represented by a set of nodes. To each node with Cartesian coordinates  $\mathbf{X}$ , we assign the Lagrange variable  $s$  as the distance along the fiber from  $\mathbf{X}$  to a reference point. The tension in the fiber obeys the generalized Hooke’s law

$$T = \tilde{T} \left( \left| \frac{\partial \mathbf{X}}{\partial s} \right| - 1 \right), \tag{11}$$

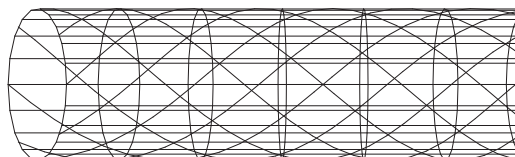


Figure 4. Set of ring, beam, and helical fibers.

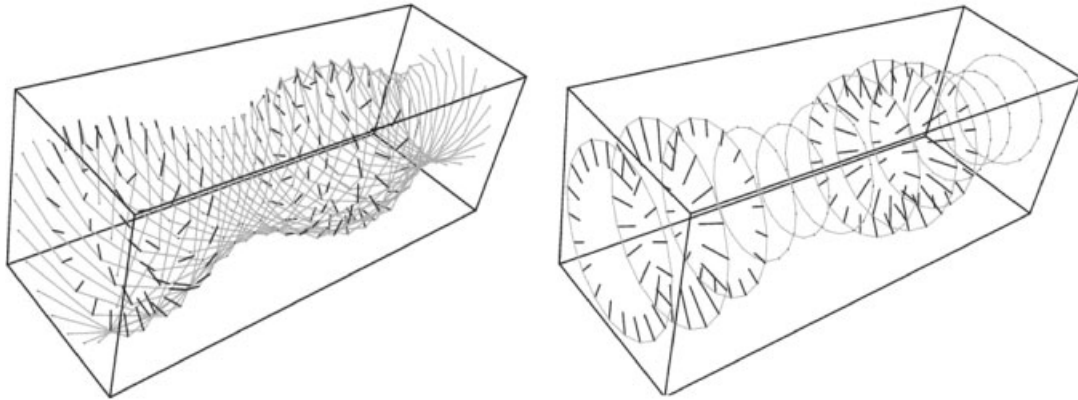


Figure 5. Forces as the response to deformation of helical fibers (left) and ring fibers (right).

where  $\tilde{T}$  is the elasticity coefficient of the fiber for  $|\partial\mathbf{X}/\partial s| \geq 1$  and  $\tilde{T} = 0$  for  $|\partial\mathbf{X}/\partial s| < 1$ . The elastic force (response to the deformation) at each node of each fiber is computed as

$$\mathbf{F} = \frac{\partial}{\partial s}(T\boldsymbol{\tau}), \quad \boldsymbol{\tau} = \frac{\partial\mathbf{X}}{\partial s} \Big/ \left| \frac{\partial\mathbf{X}}{\partial s} \right|, \tag{12}$$

where  $\boldsymbol{\tau}$  is the unit tangent to the fiber at node  $\mathbf{X}$ . In the numerical model all the derivatives are replaced with the conventional finite difference discretizations.

The composition of the nodal elastic forces  $\mathbf{F}$  forms the spatial distribution of wall response to the deformation, see Figure 5. This response can be used for different purposes. For instance, it may be interpreted as a volume force for the fluid motion, or as the counterbalance to the impact of the implant.

2.5. 3D local blood flow model

Let  $\Omega$  be a three-dimensional domain with a piecewise smooth boundary  $\partial\Omega$ . The domain is occupied by a fluid with a kinematic viscosity  $\nu$  and a density  $\rho$ . We denote by  $\mathbf{u}(\mathbf{x}, t)$  the velocity with components  $(u_1, u_2, u_3)$  and by  $p(\mathbf{x}, t) = P(\mathbf{x}, t)/\rho$  the normalized pressure of the fluid. The flow of incompressible fluid with prescribed values of the velocity on  $\partial\Omega$  obeys the Navier–Stokes equations:

$$\frac{\partial\mathbf{u}}{\partial t} - \nu\Delta\mathbf{u} + (\mathbf{u} \cdot \nabla)\mathbf{u} + \nabla p = \mathbf{f} \quad \text{in } \Omega, \quad \mathbf{u} = \mathbf{g} \quad \text{on } \partial\Omega, \tag{13}$$

$$\text{div } \mathbf{u} = 0 \quad \text{in } \Omega. \tag{14}$$

An important parameter for flow similarity is the Reynolds number  $Re = \bar{U}\bar{D}/\nu$ , where  $\bar{U}$  and  $\bar{D}$  are characteristic velocity and length, respectively. In blood flow applications, the Reynolds number varies from a fraction of one to several thousands [3]. Even within a single application, the Reynolds number can depend on particular details. For instance, an implanted filter as an obstacle has a characteristic length of 0.2 mm, whereas the filter with a caught thrombus (Figure 6) has a characteristic length of 1 cm, yielding as much as 50-fold increase of  $Re$ . This observation shows that the numerical scheme has to be robust in a wide range of Reynolds numbers.

2.6. Numerical implementation of 3D blood flow model

The time stepping scheme for the solution of unsteady equations (13)–(14) is provided by a variant of the projection algorithm (pressure correction method) [16]: given  $\mathbf{u}^k \simeq \mathbf{u}(t_0 + k\Delta t)$ , perform the steps

Step 1: Semi-Lagrangian prediction of the velocity

$$\tilde{\mathbf{u}}^{k+1} = \mathcal{L}(\mathbf{u}^k). \tag{15}$$

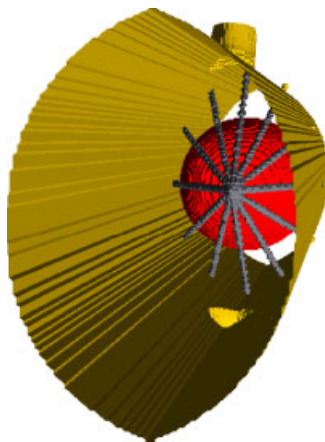


Figure 6. Example of a spherical thrombus caught by the filter.

*Step 2: Momentum equation solution*

$$\frac{\hat{\mathbf{u}}^{k+1} - \mathbf{u}^k}{\Delta t} - \nu \Delta \hat{\mathbf{u}}^{k+1} + (\tilde{\mathbf{u}}^{k+1} \cdot \nabla) \hat{\mathbf{u}}^{k+1} = \mathbf{f}^{k+1} - \nabla p^k \quad \text{in } \Omega, \quad (16)$$

$$\mathbf{u} = \mathbf{g}^{k+1} \quad \text{on } \partial\Omega$$

*Step 3: Projection of  $\hat{\mathbf{u}}^{k+1}$  onto the space of divergence-free functions by solving the elliptic equation for the pressure correction  $\delta p$*

$$-\text{div} \nabla \delta p = -\frac{1}{\Delta t} \text{div} \hat{\mathbf{u}}^{k+1}, \quad (17)$$

$$\mathbf{u}^{k+1} = \hat{\mathbf{u}}^{k+1} - \Delta t \nabla \delta p, \quad p^{k+1} = p^k + \delta p. \quad (18)$$

The numerical scheme for the approximate solution of (13) is based on the finite volume discretization of differential operators in (16)–(18). The velocity components and the pressure are assigned to staggered elements of the computational mesh. The computational mesh is the octree mesh with cut cells. The octree meshes are locally refined hierarchical meshes with cubic cells which have flexible octree structure, see Figure 7. The cut cells are formed by the intersection of the domain  $\Omega$  and the cells of the octree mesh generated in a cube containing  $\Omega$ . Each cut cell is a polyhedron since the intersection is approximated by the marching cube technique [17].

The semi-Lagrangian operator  $\mathcal{L}$  for the velocity prediction is easy to implement if the velocity were modeled as a set of particles. In this case, we would simply have to trace the particles through the given velocity field  $\mathbf{u}^k$ . To this end, we search for particles which over a single time step end up exactly at the point where each component of the predicted velocity  $\tilde{\mathbf{u}}^{k+1}$  is collocated. The values of the velocity components that these particles carry are interpolated from the neighboring collocation points for  $\mathbf{u}^k$ .

## 2.7. Multi-modeling

Interaction between the 1D, 2D, and 3D models is diverse (Figure 8). The elastic 2D wall is combined with 3D fluid flow in the framework of the fluid–structure interaction problem. The elastic 2D model is sensitive to implant installation and modifies the state equation (3) for the 1D network circulation model. The 1D network circulation model affects boundary (inflow/outflow) conditions for the 3D model, which enforces the vessel wall position and defines the pressure drop. Below we briefly comment on these ideas.

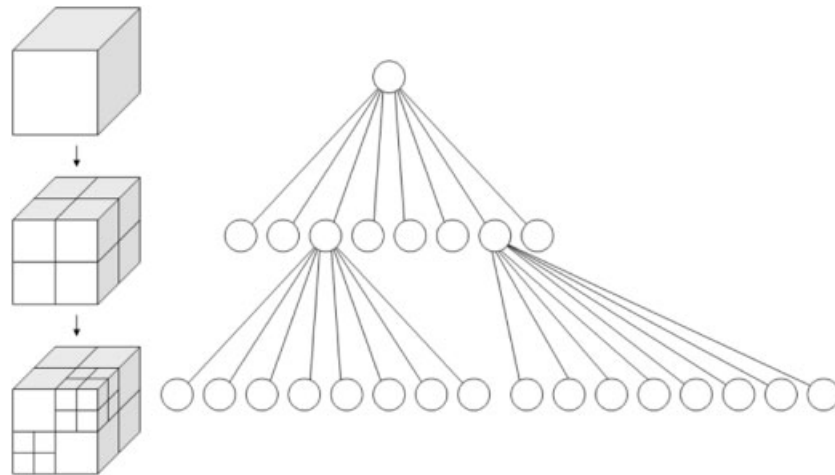


Figure 7. An octree mesh and its octree structure.

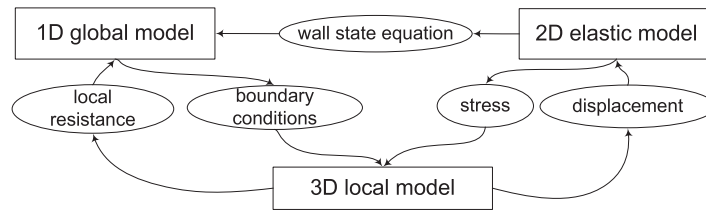


Figure 8. Multi-modeling scheme.

*Fluid–structure interaction.* The fluid–structure interaction is organized as an explicit coupling of Equations (15)–(18) and (12) via the immersed boundary method [5, 6]:

*Step I:* Perform Steps 1,2,3 of the pressure correction method and compute the new velocity field  $\mathbf{u}^{k+1}$

*Step II:* Move the elastic wall in accordance with  $\mathbf{u}^{k+1}$

$$\mathbf{X}_n^{k+1} = \mathbf{X}_n^k + \Delta t \sum_m \mathbf{u}^{k+1} \delta_h(\mathbf{x}_m - \mathbf{X}_n^k) \text{vol}(\mathbf{x}_m)$$

*Step III:* Compute fiber elastic forces

$$\mathbf{F}_n^{k+1} = \mathbf{F}_n^{k+1}(\mathbf{X}_n^{k+1})$$

*Step IV:* Interpolate the fiber elastic forces onto the fluid mesh

$$\mathbf{f}^{k+1} = \sum_n \mathbf{F}_n^{k+1} \delta_h(\mathbf{x}_m - \mathbf{X}_n^{k+1}) \text{area}(\mathbf{X}_n^{k+1})$$

Here the velocity  $\mathbf{u}^{k+1}$  defined on Eulerian fluid mesh with nodes  $\mathbf{x}_m$  is interpolated onto Lagrangian wall mesh via discrete analogues [5, 6] of the Dirac function  $\delta_h(\mathbf{x}_m - \mathbf{X}_n^k)$ , and the elastic force  $\mathbf{F}_n^{k+1}$  defined on Lagrangian mesh is interpolated onto Eulerian mesh via  $\delta_h(\mathbf{x}_m - \mathbf{X}_n^{k+1})$ . Notations vol and area stand for the representative volume and area of Eulerian and Lagrangian mesh nodes, respectively.

*Network–structure interaction.* The equation of state (3) is just the empiric qualitative description of the elastic wall properties. The drawback of such an approach is that the constant  $c_0$  should be determined for every vessel and specific formula for  $S$ -like function  $f(S)$  should be stated similar to (4). Our computational tests reveal that the flow pattern depends slightly on particular form of (4). More realistic descriptions may be given by the simulation of pressure response to

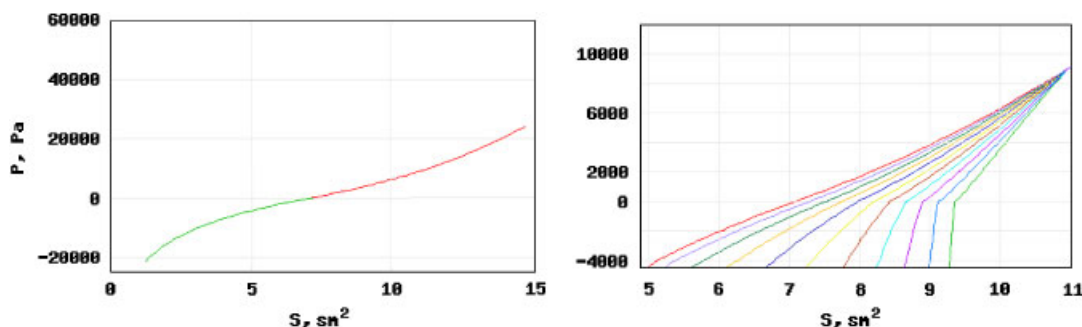


Figure 9. Equations of state for a vessel without the implant (left) and with the implant (right).

the cross-section alterations proposed in Section 2.4. It allows us to consider the elastic properties of vessels with different fiber structures of the wall's tissue as well as additional effects from endovascular implants. The output of the 2D model replaces the empiric description given by (3).

A cava filter is incorporated in the 2D elastic model as a source of expansion forces exerted at the closed curve. The curve is the intersection of the vessel and the plane passing through fixation points of filter legs, see Figure 1. The implanted filter expands the vessel and the reaction of the wall counterbalances the elastic force of filter opening. The deformed wall redistributes the strain allowing to evaluate the updated pressure and replace the equation of state (3) in the vicinity of filter implantation. We assume that the cava filter cross section cannot decrease below a given threshold. The wall reaction is evaluated in different cross sections along the axial coordinate  $x$ . This results in the set of modified wall state equations  $p(S(t, x), x)$  shown in the right picture of Figure 9 instead of the single dependence  $p(S(t, x))$  given by (3) and depicted in the left picture of Figure 9. The common point of the curves in the right picture of Figure 9 corresponds to the steady flow resulting in constant cross section along the vessel, which is equal to the cava filter cross section at the unloaded state.

We note that prior to coupling of the 1D network circulation and the 2D elastic wall model we have to calibrate the latter. The coefficients of the fiber model should be chosen so that the model recovers the conventional equation of state (3), i.e. the dependence of the transmural pressure on the area of vessel cross section shown in the left picture of Figure 9.

*Fluid–network interaction.* It is well known that the blood flow has quite a complex structure in particular parts of the vascular network, e.g. arch of aorta, in the vicinity of endovascular implants, growing clots, atherosclerotic plaques, etc. It is very difficult to provide a correct description of such flows in terms of 1D models. We suppose that regions in which 3D effects are substantial should be simulated by the 3D model coupled with the adjoining 1D regions. The 3D local fluid flow model can provide the pressure drop due to the complex flexible obstacles inside the vessel to the 1D network circulation model.

The 1D network circulation model produces the prescribed flux  $Q_i = \int_{S_i} \mathbf{u} \cdot \mathbf{n} ds$  at the ‘inlet’ and ‘outlet’ cross sections of 3D vessel-type domain  $\Omega$ . Formally, the replacement of Dirichlet data for all three velocity components with the prescribed flux data in the system (13),(14) results in not a well-posed initial-boundary value problem. However, adding to Equations (13) and (14) the extra equations for  $Q_i$  and insertion in (13) of Lagrange multipliers make the problem well-posed [7]. Moreover, the pressure correction method can be modified to solve the expanded unsteady system. The coupling of the two models within a single time step can be achieved following the approach of Quarteroni and Formaggia [3].

### 3. RESULTS

The velocity and pressure profiles along the cava vein with cava filter implanted in the middle of the vessel are shown in Figure 10. Several successive time moments with time step of 0.1

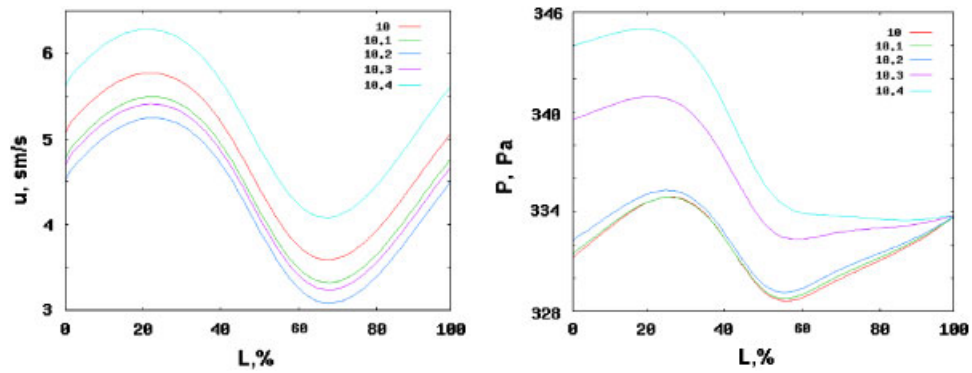


Figure 10. Velocity (left) and pressure (right) profiles along the vessel. The cava filter is placed in the middle of the vessel.

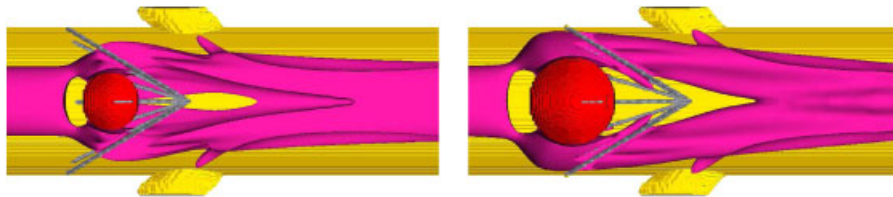


Figure 11. Region where axial velocity component is greater than 7 cm/s. The cases of spherical thrombi with diameters 0.96 and 1.44 cm are shown on left and right pictures, respectively.

second are represented. We observe the distinct pressure drop near the filter placement resulting in appropriate increase and decrease in the velocity before and after the filter. Such a flow deceleration may result in the formation of additional clots and vessel embolism. The results were obtained with the 1D network circulation model coupled with the 2D elastic wall model as stated above in the *network–structure interaction* section. The conventional wall state equation (3) is replaced here by the wall reaction simulated with the 2D elastic wall model. The initial and modified wall state equations are presented at the left and right pictures of Figure 9.

The solution of the 3D Navier–Stokes equations allows us to determine the pressure drop due to a spherical thrombus caught by the filter in situation shown in Figure 6 [18]. We consider a segment (12-cm long) of cava vein with elliptic cross section  $1.6 \times 2.4$  cm and the inlet/outlet Poiseuille-type velocity profile with maximum module 8.8 cm/s. Blood is assumed to be incompressible fluid with dynamic viscosity 0.0055 Pa s and density  $1.5 \text{ g/cm}^3$ . The clot is assumed to be a ball with diameter 0.96 or 1.44 cm. The computed pressure drops are 7 and 22 Pa, respectively. In Figure 11 we show regions where axial velocity component is greater than 7 cm/s.

#### 4. DISCUSSION

The divergent form of mass and momentum balance equations (1), (2) in the 1D network circulation model suggests the use of explicit grid-characteristic schemes of high-order (second, third) approximation [12, 14]. Locally conservative Galerkin method [13] and implicit methods are conventional for this system. Explicit formulation allows us to simplify the nonlinear system (8) for the vessel junction point. The system is characterized by a matrix of resistances and coefficients of the compatibility condition. The drawback of such an approach is the stability restriction on the time step that depends on the spatial step and the rate of small disturbance propagation in the vessel wall. The stability restriction may become substantial when rather small vessels are included in the network or the rigid wall components are considered.

We consider the *closed* network circulation model. Coupling of arterial and venous 1D networks with the dynamic heart model [14] provides a feedback from the venous part. Nevertheless, a model of the entire cardiovascular system should also include the model of micro-circulation region as it contains observable blood volume and may impact on the global circulation through different regulatory mechanisms. One possible approach to modeling flows in micro-vessels is based on the replacement of capillary and venular networks with multilayer heterogeneous porous media [19]. The other important issue in the 1D network circulation model is the reconstruction of patient-specific parameters in terms of 1D structures similar to Figures 2 and 3. It is studied thoroughly for large arteries but is still difficult to observe for the medium and small arteries and veins. Ideally, these data should be extracted from patient-specific MRI investigations.

The recovery of vessel wall state equation (3) with the 2D elastic wall model allows us to simulate the impact of different vessel abnormalities (stenosis, occlusion, clamping, wall tissue aging) on elastic properties of the vessel and therefore on the global blood circulation. The elastic wall model may be helpful in determination of the vessel shape under various values of transmural pressure as well as implant installation. This is particularly important for the recovery of the venous wall state equation as the latter is poorly approximated by (3) and other known analytic formulas. The 2D elastic wall model can be combined with other models such as the 1D network circulation or the 3D fluid flow models.

The developed 3D incompressible fluid flow model is based on the use of adaptive octree meshes with cut cells. This approach allows us to compute the interaction between small obstacles such as intravenous filters and the blood flow on a PC. The pressure correction time stepping scheme suggests a simple and effective method for fluid–structure interaction where the elastic wall motion and the fluid flow evolve simultaneously. The joint model provides evaluation of impacts of the intravenous filter onto the vessel wall such as vessel shape deformation and filter drag. The evaluation opens the way to optimization of filter design.

The developed 1D network circulation, 2D elastic wall, 3D fluid flow models will be combined in the framework of multi-model software, the endovascular computational stand. This stand is intended for the use by manufacturers and clinicians as well as the educational tool.

#### ACKNOWLEDGEMENTS

The authors want to thank T. Dobroserdova and Yu. Ivanov for the assistance in the preparation of the paper.

#### REFERENCES

1. Van de Vosse FN. Mathematical modelling of the cardiovascular system. *Journal of Engineering Mathematics* 2003; **47**:175–183.
2. Taylor CA, Draney MT. Experimental and computational methods in cardiovascular fluid mechanics. *Annual Review of Fluid Mechanics* 2004; **36**:197–231.
3. Quarteroni A, Formaggia L. Mathematical modelling and numerical simulation of the cardiovascular system. *Handbook of Numerical Analysis*, vol. XII. Elsevier: Amsterdam, 2004; 3–127.
4. Formaggia L, Quarteroni A, Veneziani A. *Cardiovascular Mathematics*, vol. 1. Springer: Heidelberg, DE, 2009.
5. Tu C, Peskin C. Stability and instability in the computation of flows with moving immersed boundaries: a comparison of three methods. *SIAM Journal on Scientific and Statistical Computing* 1992; **13**(6):1361–1376.
6. Rosar M, Peskin C. Fluid flow in collapsible elastic tubes: a three-dimensional numerical model. *New York Journal of Mathematics* 2001; **7**:281–302.
7. Formaggia L, Gerbeau J-F, Nobile F, Quarteroni A. Numerical treatment of defective boundary conditions for Navier–Stokes equations. *SIAM Journal on Numerical Analysis* 2002; **40**(1):376–401.
8. Huang W, Yen RT, McLaurine M, Bledsoe G. Morphometry of the human pulmonary vasculature. *Journal of Applied Physiology* 1996; **81**(5):2123–2133.
9. Huang W, Yen RT. Zero-stress states of human pulmonary arteries and veins. *Journal of Applied Physiology* 1998; **85**(3):867–873.
10. Gray H. *Gray's Anatomy: The Anatomical Basis of Medicine and Surgery* (39th edn). Churchill-Livingstone: London, 2004.
11. Schmidt RF, Thews G. *Human Physiology* (2nd edn), vol. 2. Springer: Berlin, 1989.
12. Simakov SS, Kholodov AS, Kholodov YA *et al.* Global dynamical model of the cardiovascular system. *Proceedings of the III European Conference on Computational Mechanics*, 2006; 1467.1–1467.15.

13. Mynard JP, Nithiarasu P. A 1D arterial blood flow model incorporating ventricular pressure, aortic valve and regional coronary flow using the locally conservative Galerkin (LCG) method. *Communications in Numerical Methods in Engineering* 2008; **24**(5):367–417.
14. Simakov SS, Kholodov AS. Computational study of oxygen concentration in human blood under low frequency disturbances. *Mathematical Models and Computer Simulations* 2009; **1**(2):283–295.
15. Pedley TJ, Luo XY. Modelling flow and oscillations in collapsible tubes. *Theoretical and Computational Fluid Dynamics* 1998; **10**(1–4):277–294.
16. Marion M, Temam R. Navier–Stokes equations: theory and approximation. *Handbook of Numerical Analysis*, vol. VI. Elsevier: Amsterdam, 1998; 503–689.
17. Lorensen W, Cline H. Marching cubes: a high resolution 3D surface construction algorithm. *Computer Graphics* 1987; **21**(4):163–169.
18. Vassilevski YV, Kapranov SA. Parallel modeling of blood flow peculiarities in the vicinity of cava filter with captured clot. *Mathematical Modeling* 2005; **17**(11):3–15.
19. Kholodov AS, Evdokimov AV, Simakov SS. Numerical simulation of peripheral circulation and substance transfer with 2D models. In *Mathematical Biology*, Chandra P, Kumar R (eds). Anamaya Publishers: New Delhi, 2006; 22–29.